

Interannual Variability of the Antarctic Ozone Hole in a GCM. Part I: The Influence of Tropospheric Wave Variability

DREW T. SHINDELL,* SUN WONG,* AND DAVID RIND

NASA/Goddard Institute for Space Studies, New York, New York

(Manuscript received 12 November 1996, in final form 17 March 1997)

ABSTRACT

To study the interannual variability of the Antarctic ozone hole, a physically realistic parameterization of the chemistry responsible for severe polar ozone loss has been included in the GISS GCM. The ensuing ozone hole agrees well with observations, as do modeled surface UV increases of up to 42%. The presence of the ozone hole causes a reduction in lower stratospheric solar heating and an increase in upper stratospheric descent and dynamical heating in the model, as expected. Both the degree of ozone depletion and the dynamical response exhibit large interannual variability, however. These variations are driven by differences in the midwinter buildup of tropospheric wave energy in the model, which affect the dynamics globally for several months according to the mechanism detailed herein. Starting by July, strong tropospheric wave activity leads to greater energy reaching the lower stratosphere, and therefore warmer temperatures, than in years with weak wave activity. The warmer temperatures persist throughout the austral spring, resulting in ozone losses that are only ~80% of those seen in the years with weaker wave activity. Significant differences also occur in the zonal wind field, setting up conditions that ultimately affect the propagation of wave energy in the spring. Differences in the propagation of wave energy lead to an October increase in upper stratospheric dynamical heating that is more than three times larger in the years with weak wave activity than in years with strong wave activity. Modeled interannual variations in both upper stratospheric temperatures and ozone loss are of similar magnitude to observations, though the largest observed variations exceed those seen here, indicating that unforced variability likely plays a significant role in addition to periodic forcings such as the QBO. The results are in accord with observational studies showing a strong anticorrelation between the interannual variability of tropospheric wave forcing and of the Antarctic ozone hole, suggesting that midwinter tropospheric wave energy may be the best predictor of the severity of the ozone hole the following spring.

1. Introduction

The annual springtime ozone hole over Antarctica is one of the largest anthropogenic perturbations to the atmosphere. While there has been much progress in recent years in understanding the chemical mechanisms responsible for the severe ozone depletion, the impact of the ozone hole on atmospheric radiation and dynamics is less well understood. Though several studies have been done (Kiehl et al. 1988; Cariolle et al. 1990; Mahlman et al. 1994), many questions about the induced dynamical changes and especially about the causes of the interannual variability of the ozone hole remain unresolved.

To investigate the radiative and dynamical impacts of

the chemical ozone hole, we have included parameterized polar heterogeneous chemistry in the Goddard Institute for Space Studies (GISS) Global Climate Model (GCM). A full three-dimensional model such as this is necessary to properly simulate planetary wave propagation. The use of parameterized chemistry allows for relatively rapid simulations, even with the detailed treatment of dynamics and radiation included in the climate model, so that we can perform multiyear experiments to investigate the interannual variability of the ozone hole. Interannual variability is due to interactions between planetary waves, the mean circulation, and gravity wave drag. The GCM does not produce a quasi-biennial oscillation (QBO). However, the magnitude of the unforced variations that occur in the model is in reasonable agreement with observations at extratropical latitudes (Rind et al. 1988b). We will focus here on examining the interaction between dynamics and chemistry in order to better understand the mechanism whereby planetary waves affect the development of the Antarctic ozone hole. The respective influence of period forcing versus unforced variability will be addressed in a forthcoming paper, Part II of this series.

*Also affiliated: Center for Climate Systems Research, Columbia University, New York, New York

Corresponding author address: Dr. Drew T. Shindell, NASA GISS, 2880 Broadway, New York, NY 10025.
E-mail: dshindell@giss.nasa.gov

2. Model design

A physically realistic parameterization of the heterogeneous chemistry responsible for polar ozone depletion was included directly into the 23-layer GISS GCM (Rind et al. 1988a,b). This model has 23 vertical layers extending from the surface to 85 km, with $8^\circ \times 10^\circ$ horizontal resolution. It is a primitive equation model that includes parameterized gravity waves. For both the control and ozone loss runs, the model was run with one-quarter the amount of mountain drag normally used. This gives a good reproduction of observed temperatures in the southern polar lower stratosphere, which are otherwise too warm. Reducing the drag does marginally reduce the quality of the simulation at other latitudes, however.

In the chemistry parameterization, we calculate the fraction of available chlorine activated into chlorine monoxide at each point, based upon the modeling of Shindell and de Zafra (1996, 1997). Total chlorine in the model is set to early 1990s atmospheric loading. Whenever temperatures are cold enough for polar stratospheric clouds (PSCs) to form, full activation takes place in five hours. Deactivation is a function of elapsed sunlit time since the last exposure to PSCs. The amount of chlorine monoxide decreases linearly to zero in 80 sunlit hours, following the deactivation rate seen in the one-dimensional modeling. Since ozone depletion depends on the square of the chlorine monoxide abundance, from the rate limiting reaction $\text{ClO} + \text{ClO} + M \rightarrow \text{Cl}_2\text{O}_2 + M$, the neglect of a slight deactivation tail seen in the one-dimensional modeling is insignificant. Ozone depletion takes place at each point in the GCM where sunlight and active chlorine are present simultaneously. Ozone loss is calculated according to $d[\text{O}_3]/dt = -2k[\text{ClO}]^2[M]$, where $[\text{ClO}]$ is the concentration of chlorine monoxide, k is the temperature dependent rate constant of the ClO dimer formation reaction given above, and $[M]$ is the concentration of background gas molecules. We also include an additional contribution of $\sim 15\%$ from bromine chemistry. Transport of depleted ozone was not included in these experiments. Since we are primarily concerned with the Southern Hemisphere, where springtime ozone loss is well constrained within the strong polar vortex, this should not greatly influence our results. Of course, transport of air containing depleted ozone to middle latitudes after the breakup of the polar vortex will not occur in these experiments. Ozone is relaxed to climatological values as a function of latitude. Ozone recovery rates are parameterized so that ozone losses are restored based on the photochemical lifetime of ozone at each altitude, as calculated in the one-dimensional model for every 5° latitude. In practice, rates that are slightly faster than the purely photochemical rates are used. These have been chosen to reproduce the observed behavior, which includes transport to lower latitudes where recovery is more rapid. Severe ozone depletion therefore persists in the model for approxi-

mately the same time as in observations, though the actual date of recovery of ozone to a particular value of course varies with the timing of the final warming and breakup of the polar vortex. All impacts of the ozone hole are assessed relative to a 5-yr control run.

3. Simulated ozone hole

We find that the ozone depletion produced with the on-line parameterization is quite similar to that produced in the one-dimensional chemistry model when that model is run interactively (but off-line) with the GCM. While the off-line calculations include full chemistry at each point, they are very time consuming, so we were able to perform a much longer run using the parameterized on-line chemistry. We therefore focus on the results of that run, as they give a better picture of long-term dynamical impacts of the ozone hole and of interannual variability.

We have run the GCM with parameterized PSC chemistry for 6 years. Despite the simple chemistry and lack of ozone loss transport in this experiment, calculated Antarctic ozone losses are in fairly good quantitative agreement with observations (e.g., Waters et al. 1993). This was also the case in the earlier GCM experiment of Cariolle et al. (1990), which used a similar parameterization for polar heterogeneous chemistry. The results divide into two distinct groups based on the ozone depletion that takes place, which we will call the large loss (years 1, 3, and 6) and small loss (years 2, 4, and 5) groups to differentiate between them. Figure 1 gives zonal mean vertical profiles of net ozone loss at the end of September for the two groups. The most severe ozone losses extend to higher altitudes and to lower latitudes in the large-loss group than in the small-loss group. These differences are quite apparent in Figs. 2 and 3, which show the springtime evolution of ozone loss in the layers centered at 32 and 68 mb for year 1, the largest loss year, and year 4, the smallest loss year. By the end of September, the ozone decrease in a large loss year is up to 18% greater in the GCM layer centered at 68 mb and up to 71% greater in the one centered at 32 mb than in a small loss year. Differences in the geographical area of ozone loss can be seen clearly at the end of September in the layer centered at 68 mb. In the small loss year, significant ozone depletion remains largely confined to poleward of about 65°S , while in the large loss year, ozone losses of 10% are seen as far north as the southern tip of South America.

The general features of the observed development of the ozone hole are well reproduced. Ozone depletion extends gradually farther south during the spring as sunlight returns to the polar region. Temperatures in the GCM are typically coldest just eastward of the Antarctic Peninsula, as a result of mountain lee wave effects, in good agreement with observations (World Meteorological Organization 1994). This leads to a maximum in ozone loss in that region, though this phenomenon

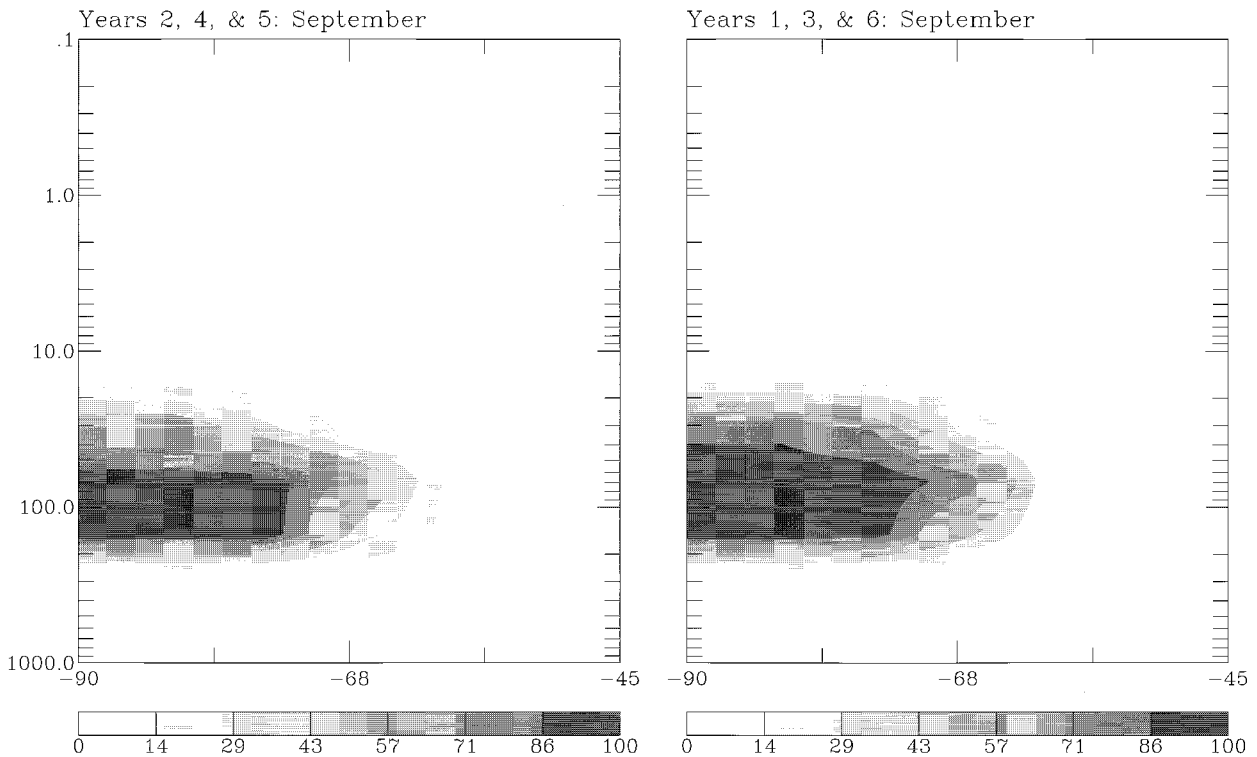


FIG. 1. Net zonal-mean ozone loss at the end of September in percent during the indicated years due to catalytic destruction when parameterized polar stratospheric cloud formation and heterogeneous chemistry are included in the GCM.

would also be influenced by transport. Maximum losses occur in the month of October in both the model and observations. Active ozone depletion also ceases during October as temperatures rise past the PSC threshold. The earlier temperature rise and faster recovery of ozone at high altitudes can be seen by comparing Figs. 2 and 3. At the end of October, ozone has recovered significantly in the 32-mb layer where the photochemical lifetime of ozone is shorter. The depletion relative to the climatological value is less than half the amount that was present at the end of September, while in contrast the depletion is still quite large in the 68-mb layer, though somewhat reduced from the mid-October maximum.

4. Radiative and dynamical impacts

The radiative impact of the ozone hole is closely correlated to the column ozone loss in the model, both of which show interannual variations of $\sim 20\%$. In both the large loss and small loss groups of results, the depletion of ozone in the lower stratosphere causes a reduction in the absorption of solar radiation there and a corresponding increase in the outgoing radiation absorbed at higher altitudes. The resulting changes in solar heating differ by $\sim 20\%$ between the two groups, in accordance with the differences in ozone depletion in the two groups. We find a maximum reduction in lower

stratospheric solar heating of 1.24 K d^{-1} in the small loss group average versus a maximum of 1.49 K d^{-1} in the large loss group average—a 20% difference. In the upper stratosphere, the increased absorption leads to a maximum increase in solar heating of 0.17 K d^{-1} in the small loss group average. The maximum is 0.20 K d^{-1} in the large loss group average, 18% greater than in the small-loss cases. These results are shown in Fig. 4 for October, when the monthly mean ozone depletion is greatest. Note that the most significant heating differences occur near the top of the area of severe depletion at around 30–40 mb, where the ozone depletion is most different between the two groups (as shown in Figs. 1 and 2).

The ozone losses also impact the amount of potentially harmful ultraviolet (UV) flux reaching the earth's surface. We find a zonal mean increase in UV radiation incident at the surface of 24% from 55° to 70°S during November, with a maximum zonal mean increase of 42% near the outer edge of the ozone hole in large-loss years. The latter results are in good agreement with observations of a 45% increase in 306.5-nm flux taken in December at 55°S , near the tip of South America (Frederick et al. 1993).

There is a strong correlation between the variations in ozone loss and the dynamical response in our model as well. The dynamical changes show much larger in-

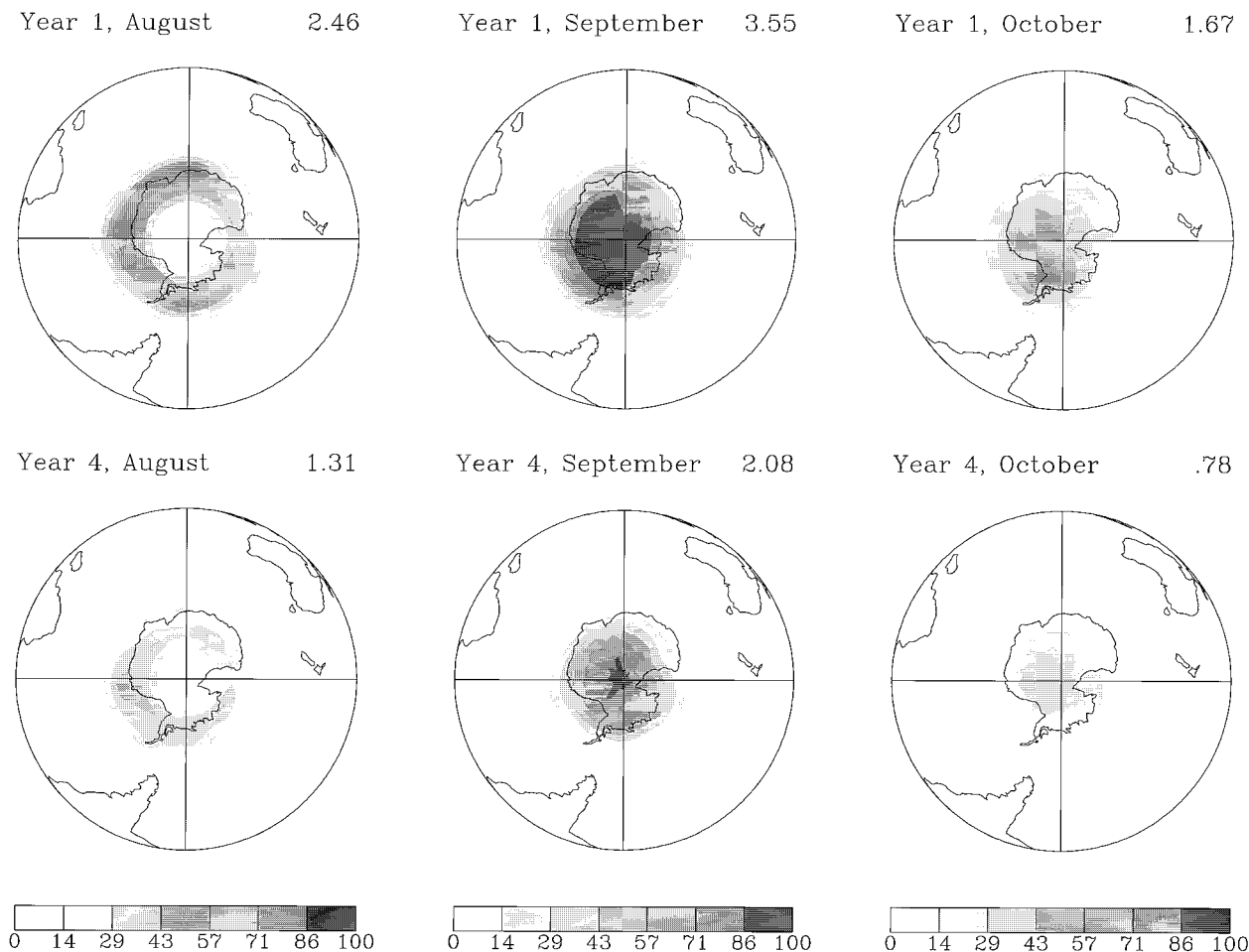


FIG. 2. Percentage ozone loss in the layer, ~ 5 km thick, centered at 32 mb during the austral spring for the largest ozone loss (year 1) and the smallest ozone loss (year 4) years. Losses are given for the end of the indicated months. The number in the upper right-hand corner of each plot is the global mean percentage ozone loss in the layer, which is useful for comparison of the two years.

terannual variations than those seen in ozone loss or in the radiative response, however; increases in dynamical heating due to the ozone hole vary by up to a factor of 3 between the two groups. We first discuss the general features of the dynamical response to an ozone hole in the GCM.

In both groups, the October zonal wind from 50° to 80° S increases relative to the control runs from about 200 to 1 mb. This increase is consistent with the increased latitudinal temperature gradient arising from the decreased solar heating in the polar lower stratosphere (as shown in Fig. 4). The faster zonal winds lead to a stronger polar vortex and an increased descent rate of the high latitude residual circulation, causing dynamical heating of the upper stratosphere, as shown in Fig. 5. The magnitude of the induced heating is quite different in the two groups, however. In the small-loss group average, dynamical heating increases by up to 0.78 K d^{-1} relative to the control run. In the larger-loss group average, the maximum increase is 2.5 K d^{-1} , more than

three times greater. The zonal wind increases exhibit a similar variation. Note that, in either case, the dynamical heating increases clearly dominate over the radiative heating increases in this region. We now examine the differences between the two groups.

5. Sources of interannual variability

We find that interannual variability in ozone loss and dynamical forcing is associated with variations in planetary wave energy in our model. These energy variations manifest themselves well before large amounts of ozone loss or increases in dynamical heating take place. Significant interannual differences in tropospheric wave energy are already apparent in July in our experiments. Table 1 gives the mean kinetic energy in the Southern Hemisphere for wavenumber one and for total eddy energy, for both the control run and the ozone hole run. The large-loss years 1, 3, and 6 have much weaker wave energies than the small loss years 2, 4, and 5. For il-

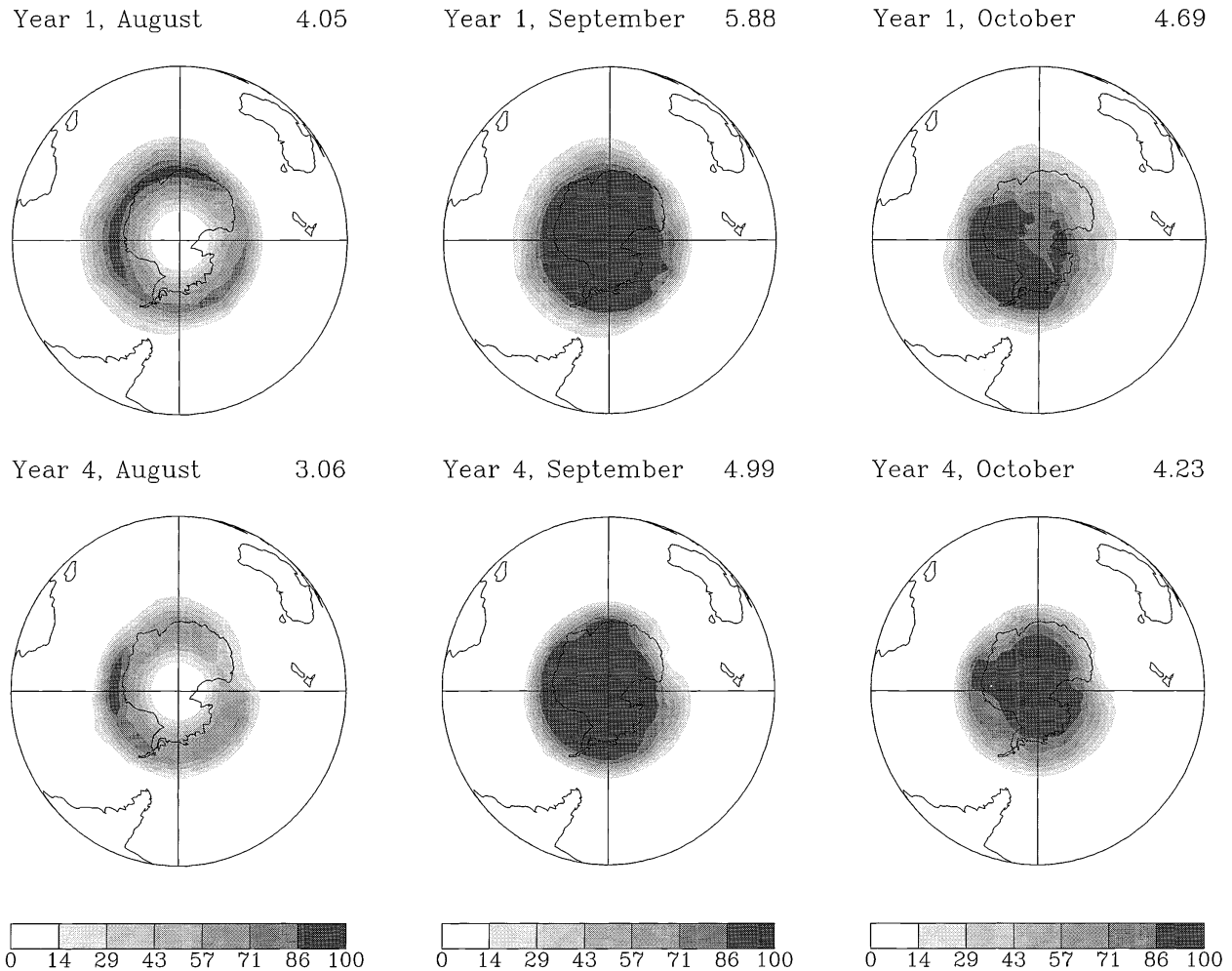


FIG. 3. As in Fig. 2 but for the layer, ~ 5 km thick, centered at 68 mb.

illustrative purposes, we will focus on the most extreme years of each group, year 1 for the large-loss case and year 4 for the small loss case, and on October, when the ozone depletion was greatest.

Both the dynamical heating and ozone loss differences between years 1 and 4 arise from differences in the degree to which tropospheric wave energy is able to propagate into the stratosphere. In an example of the coupling between dynamics and chemistry, the variations in planetary wave propagation affect temperatures and thereby influence the amount of ozone loss. A greater amount of dynamical warming takes place in the lower stratosphere in the small-loss cases (strong wave activity) than in the large loss cases (weak wave activity) in July and August, when the refractive indices for wave propagation are similar, as there is simply more available energy. Zonal mean temperatures at southern high latitudes are given in Table 2 for years 1 and 4. The greatest temperature differences occur in August and September, which are the prime months for ozone depletion. Zonal

mean temperatures at or below the PSC formation threshold of 195 K are highlighted in bold type in Table 2. They occur significantly more often in the large-loss year.

The colder temperatures and resulting greater abundance of PSCs in the large-loss years leads to greater ozone destruction. The largest effects are seen near the edges of the ozone hole at higher altitudes and lower latitudes where temperatures are very close to the threshold value, rather than in the region of most severe depletion where temperatures are typically below the PSC threshold in all years. Thus the primary change of ozone loss is in its vertical and horizontal extent, rather than in the magnitude of depletion in the center of the ozone hole, as seen in Fig. 1. At 32 mb, for example, the ozone loss in the largest loss year is nearly twice that of the smallest loss year, as was shown in Fig. 2.

Interannual variations in dynamical heating after August also result from differences in tropospheric wave activity. Strong wave activity sets up an increased equa-

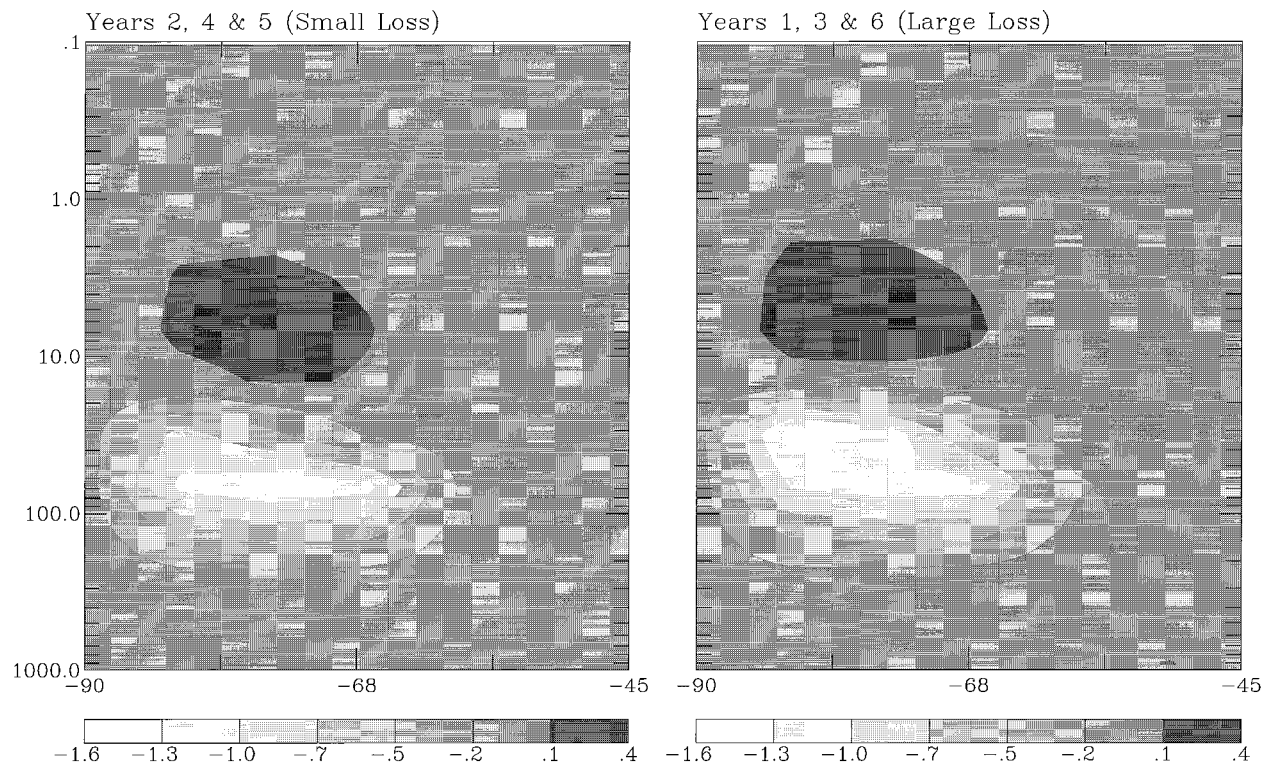


FIG. 4. October-mean change in solar heating (in $K d^{-1}$) due to the ozone hole. Zonal-average differences between the 5-yr average of the control run (without an ozone hole) and the indicated years of the ozone hole runs are shown.

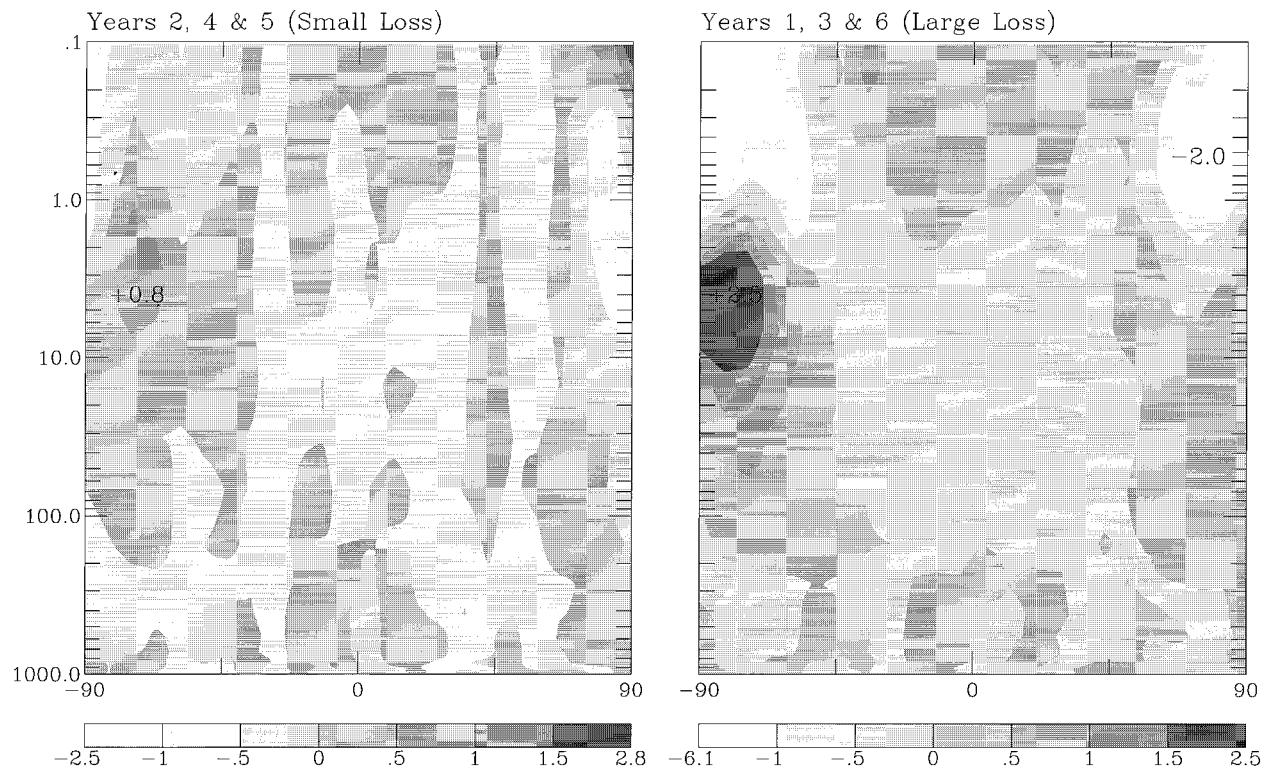


FIG. 5. As in Fig. 4 but for dynamical heating. Note that the latitude scale is now global.

TABLE 1. July Southern Hemisphere tropospheric kinetic energy (10^{17} J).

		Run					
		1	2	3	4	5	6
Control:	Wave one	307	344	313	319	382	
	Total eddy	2644	2615	2711	2679	2728	
Ozone hole:	Wave one	233	341	311	347	321	289
	Total eddy	2512	2839	2679	2853	2774	2561

torward flow in the GCM, doubling the Eliassen–Palm (EP) flux convergence at low and midlatitudes near the tropopause in year 4 (small loss) relative to year 1 (large loss). This reduces the zonal wind at these levels, especially at the subtropical jet, as shown in Table 3. This pattern is initially set up in July during the polar winter but persists throughout the austral spring, as seen in Table 3. In fact, the zonal wind values for the two years diverge most sharply during September and October. The zonal wind shear gradients are also different, influencing the propagation of tropospheric waves. While the refractive indices for wave propagation ($-d^2u/dy^2$) near the tropopause are large in August in both years, differences in dynamical heating are due simply to differences in available energy. By October, however, the refractive index has become very small in the large-loss case (year 1), while it remains large in the small loss case (year 4). Tropospheric wave energy is therefore more often refracted in the small loss years and tends to propagate northward instead of upward in the late spring, following the flow pattern set up in mid winter. In contrast, in the large loss years, a great deal of eddy energy reaches the stratosphere, causing the large dynamical heating that was shown in Fig. 5. While there is a qualitatively similar difference in tropospheric wave activity forcing of the stratosphere between the control run years with weak and strong wave energies, it is much smaller. In the control run, the dynamical heating rate is $\sim 20\%$ larger in October in the years with weak wave energy, while in the ozone hole runs it is $\sim 70\%$ larger. Thus the presence of the ozone hole seems to greatly amplify differences in wave propagation, perhaps via the ozone hole's increase of the zonal wind at lower latitudes.

After August, wave propagation into the stratosphere

TABLE 2. Zonal average temperatures at 32 mb (K). Temperatures at or below the PSC formation threshold in bold.

	Latitude	Jul	Aug	Sep	Oct
Year 1					
(Large loss)	67°S	199	195	200	212
	74°S	195	192	194	205
	82°S	193	189	191	202
Year 4					
(Small loss)	67°S	200	207	201	209
	74°S	195	199	197	205
	82°S	192	193	193	201

is much greater in the large-loss cases, as discussed above, leading to much more dynamical heating. While the reduced solar heating due to the greater degree of ozone loss (see Fig. 4) does compensate for some of the greater dynamical heating in the large loss years, it is a smaller effect so that the lower stratospheric temperatures rise more quickly in the large-loss years. Despite the rapid increase of temperatures in those years, they do not catch up to the warmer temperatures found in the small loss years until October, as seen in Table 2. The net results of the radiative and dynamical heating changes in October are the temperature changes shown in Fig. 6. There is a warming of up to $+20$ K in the polar upper stratosphere in the large ozone loss cases and a smaller cooling in the lower stratosphere, up to -6 K, both relative to the control run with no ozone hole. Though the wave energies in the six ozone hole years cover a wide range, the results in Fig. 6 fall distinctly into two categories, implying that the overall response varies nonlinearly with wave energy. Even years 3 and 5, which are quite close in wave energy, are quite different in their responses, indicating that the threshold energy is somewhere between these two cases.

Ozone depletion in general enhances dynamical variability, with cooling due to ozone reductions acting as a positive feedback on the strength of the polar vortex. The interannual dynamical heating differences are the cause of the interannual ozone loss differences however, and not vice versa. Interannual variability of winter tropospheric wave activity sets up an altered pattern for the propagation of wave energy, creating these heating differences and thereby exerting a significant influence on the amount of ozone loss in the GCM.

6. Extended temporal and spatial impacts

In November, the warming of the upper stratosphere has reduced by about half in the large loss years, while the lower stratospheric cooling remains about the same.

TABLE 3. Maximum zonal wind at southern subtropical jet ($m\ s^{-1}$).

	Jul	Aug	Sep	Oct
Year 1 (large loss, weak wave energy)	41.3	39.9	40.7	34.7
Year 4 (small loss, strong wave energy)	39.8	36.7	31.7	28.7

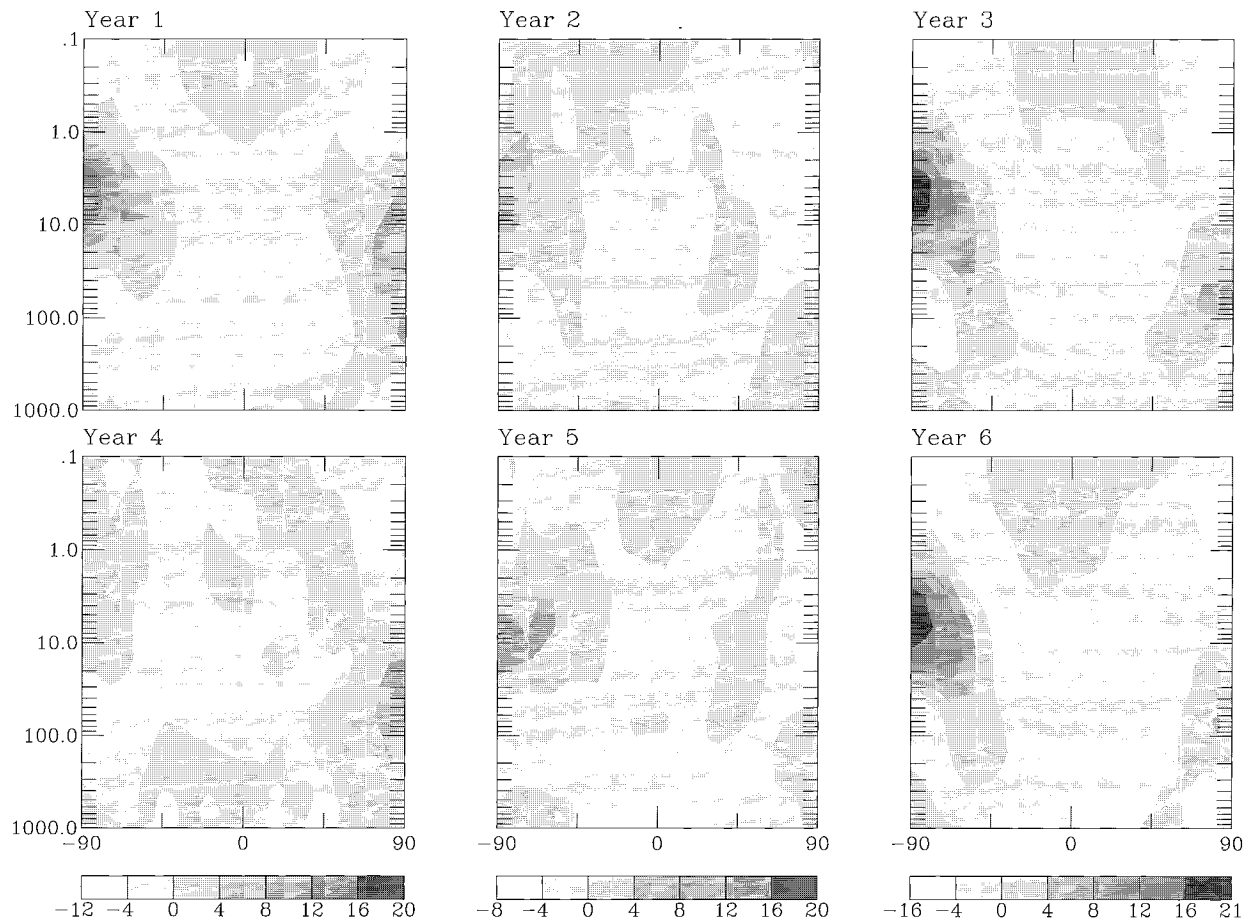


FIG. 6. October-mean zonal-average temperature differences between the six individual years of the ozone hole run and the average of the 5-yr control run. The results fall clearly into two groups (1, 3, and 6 and 2, 4, and 5), as discussed in the text.

In the small loss years though, the cooling in the lower stratosphere has increased to about -10 K from 50 to 100 mb. December exhibits no statistically significant temperature changes in the large loss years in the Southern Hemisphere, as the dynamical heating has fully compensated for the cooling from ozone loss. Traces of the lower stratospheric cooling caused by the Antarctic ozone hole persist until April in the small loss years, however, but are not statistically significant after February. The large dynamical heating of the upper stratosphere in the large loss cases greatly reduces the latitudinal temperature gradient, causing a reduction in the high altitude (<30 mb) zonal wind by November, in contrast to the continued increase relative to the control run seen in the small loss years. Thus we tend to see an earlier breakup of the polar vortex at high altitudes in the large loss years relative to the small-loss years. In the lower stratosphere, the final warming of the vortex has been substantially delayed by the formation of the ozone hole in all years, though especially in the small loss years, as indicated by the large coolings that remain through November and December.

We also find that the Antarctic ozone hole induces statistically significant temperature changes at high northern latitudes in the large loss years. From October to March, there is a warming of ~ 4 – 10 K in the lower stratosphere at latitudes above $\sim 70^\circ\text{N}$, accompanied by a cooling of approximately -6 to -12 K in the upper stratosphere, peaking at ~ 1.0 mb. A similar cooling of -6 to -8 K at ~ 0.5 mb was seen in December in the experiment of Mahlman et al. (1994), though it was not statistically significant and was unaccompanied by a lower stratospheric warming. Mean values of temperature changes for December through February are shown in Fig. 7. The only statistically significant changes are those at high northern latitudes in the large loss years and the lower stratospheric cooling at high southern latitudes in the small loss years. We attribute the Northern Hemisphere changes to changes in the large-scale circulation induced by the ozone hole, though given the complexity of Northern Hemisphere dynamics, it is difficult to see precisely how the changes are connected. A dynamical warming takes place at high northern latitudes in the middle and lower stratosphere

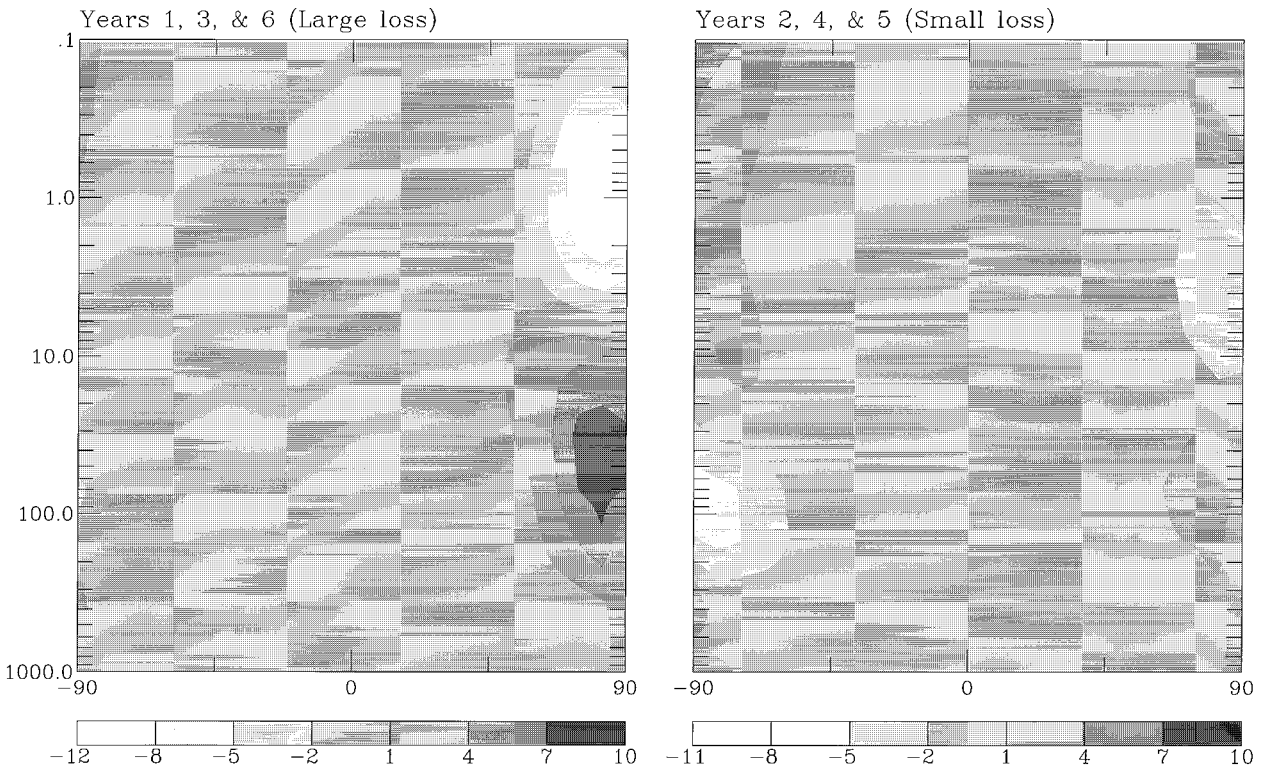


FIG. 7. Mean values of temperature changes induced by the ozone hole for December through February averaged over the indicated years. Note that zero is not at a grayscale bar division, to reduce the visibility of statistically insignificant small changes.

due to an increase in eddy energy convergence. This warming reduces the latitudinal temperature gradient, leading to a reduction in the zonal wind speed. This effect is opposite to what happens in the Southern Hemisphere, where an increase in the latitudinal temperature gradient causes the high latitude zonal wind speed to increase. Significant reductions in the Northern Hemisphere zonal wind in the middle stratosphere begin in October. For example, at 30 mb, there are mean decreases of 10 and 14 m s^{-1} in the large loss years during October and November, respectively. We note that in the small loss years, decreases of 3 and 5 m s^{-1} are seen during those months, showing a similar trend although of much weaker strength. In summary, we see a general increase in the rate of heating due to eddy convergence at high northern latitudes, leading to warming in the middle and lower stratosphere, accompanied by a cooling in the upper stratosphere due to a reduction in the mean circulation in the Northern Hemisphere. Thus we see the opposite pattern of temperature changes in the north, with dynamical cooling at high altitudes and warming lower down. The rather surprising implication of this result is that the presence of a large Antarctic ozone hole may be causing a warming of 3–7 K in the Arctic lower stratosphere during March and April, when PSC formation takes place there. Thus greater Antarctic ozone loss may possibly lead to reduced Arctic ozone

loss. Given the high degree of variability of planetary waves in the Northern Hemisphere, however, it seems unlikely that a significant correlation could be established in observations or that such a correlation could be used for predictions of Arctic ozone losses. Additionally, the lack of changes in ozone transport in our model may affect the results.

7. Comparison of response and variability with observations and other models

Earlier GCM experiments found mostly similar magnitudes of temperature responses to the Antarctic ozone hole, as shown in Table 4. Results presented here from other models are approximate maximum values derived from figures available in their publications. Observations are the single year values reported by Randel (1988) for 1987 relative to the 1980–86 mean. The models all found a maximum zonal mean cooling of 4 to 8 K in the lower stratosphere in October, in good agreement with the observations. In the upper stratosphere, Kiehl et al. (1988) and Cariolle et al. (1990) found warmings of 4 K, similar to the 5 K warming seen in the small loss years of our runs and, again, in accord with observations. They did not show warmings as large as the +20 K seen in our large loss years; however, their experiments were each only a single year (as were

TABLE 4. Modeled maximum stratospheric temperature variations (K).

	Our model	Kiehl	Mahlman	Cariolle	Obs (1987)
October lower stratosphere	-4 to -8	-6	-4 to -8	-7	-6
October upper stratosphere	+5 (small loss) +20 (large loss)	+4	Not shown	+4	+4
November lower stratosphere	0 to -12	-6	-7 to -11	-15	-14
November upper stratosphere	+5 to +7	+6	Not shown	+5	+6

the observations). Mahlman et al. (1994) do not show upper stratospheric temperature changes for October or November.

In November, we find a cooling in the lower stratosphere ranging from 0 to -12 K. Our mean value is -6 K, which includes a year in which there was no cooling, as the final warming came quite early. Without that year, the mean cooling was -8 K, similar to the range of results from other models. The single year observation is at the high end of the model results and may furthermore be an underestimate of temperature change due to the ozone hole since 1980-86 did include some ozone depletion. In the November upper stratosphere, our model results are in good agreement with the other models and with the 1987 observations.

The largest interannual variations in temperature in our model are the 12-16 K variations in the polar upper stratosphere. National Meteorological Center (now the National Centers for Environmental Prediction) compilations of observational data show approximately a 15 K range of monthly mean temperatures at 5 mb during Octobers from 1985 to 1990, in good agreement with our results. Earlier model experiments did not strongly focus on interannual variability, however. Interannual variation could not be studied in the single year run of Cariolle et al. (1990). In the multiyear experiment of Mahlman et al. (1994), the lower stratospheric temperature response varies by ~20% interannually, in good agreement with our results there, but they do not discuss interannual variations in the upper stratospheric response. Kiehl et al. (1988) give explicit results for only a single year ozone hole run with the NCAR GCM but do note that in the second year of that run the amount of the dynamical warming in the upper stratosphere (1-10 mb) changed by a factor of 2, suggesting large interannual variability such as that seen in our model.

The maximum interannual variation in total column ozone loss is ~25% in the six years of our ozone hole experiment, with typical variations of ~15%. Observations show typical interannual variations in column ozone loss of ~15%-25%, with a maximum change that was considerably larger (>50%) between 1987 and 1988 (World Meteorological Organization 1994), indicating that observed variability is of a similar degree to, though sometimes significantly greater than, the unforced model variability.

8. Correlations between wave energy and ozone loss

The link between planetary wave energy and the severity of the Antarctic ozone hole has been examined in several observational and modeling studies. Bodeker and Scourfield (1995) find a strong anticorrelation between Southern Hemisphere midlatitude total wave power and the severity of Antarctic ozone loss using Total Ozone Mapping Spectrometer (TOMS) data. Total wave power is primarily from wavenumber one, so the anticorrelation holds true for wave 1 and ozone loss as well. Furthermore, the best correlation was obtained when a time lag of approximately 2 months between wave energy and ozone loss was used (G. Bodeker 1996, personal communication). This supports our results, indicating that it is the midwinter wave energy which is critical in determining the ozone loss behavior in the springtime, approximately 2 months later. Kawahira and Shiratori (1996) have performed a somewhat different analysis of TOMS data and also find an anticorrelation between wave power and ozone loss. It should be noted that both of these studies suggest that the correlation of wave power with ozone loss becomes much weaker during 1991 and 1992, the last two years included in those studies, perhaps due to chlorine saturation, volcanic effects, or changes in wave structure. Using a three-dimensional model with prescribed wave energy forcings at its lower boundary, Austin and Butchart (1992) also found a strong anticorrelation between the amplitude of the prescribed wave forcing and the degree of ozone loss. Thus, the observational and modeling studies provide strong evidence for an anticorrelation between tropospheric wave energy and ozone depletion taking place by the mechanism elaborated herein.

The source of the variations in tropospheric wave forcing is less well understood, however. As shown in Balachandran and Rind (1995) and Rind et al. (1988b), the natural variability of wave activity in the GISS GCM reproduces observed variability of extratropical zonal winds quite well. The reduction in mountain drag in these runs does affect the variability of tropospheric wave energy, but not hugely. The standard deviation in the July Southern Hemisphere total eddy energy is reduced from $\sim 65 \times 10^{17}$ J to $\sim 50 \times 10^{17}$ J, so the variability seen here may somewhat underestimate that

in the real world. We also find that tropospheric wave variability greatly increases with the presence of a seasonal ozone hole, to a standard deviation of $\sim 140 \times 10^{17}$ J. It is not clear how this feedback takes place, however. Observations also show increased variability in the period 1985–92 relative to the pre-ozone hole period 1979–85 (Bodeker and Scourfield 1995; Kawahira and Shiratori 1996). However, the phase of the QBO and the solar UV cycle may also effect variations in wave energy over time in the atmosphere so that we cannot conclusively connect the observed increase in wave variability to the appearance of the ozone hole.

Variations in wave energy due to forcings such as the QBO could also affect ozone loss. In Balachandran and Rind (1995), the inclusion of a QBO in the GISS GCM did change temperatures at high southern latitudes. We will address this issue in a forthcoming publication, Part II of this series. At present we note that Bodeker and Scourfield (1995) discuss observations of a correlation between the QBO in equatorial winds and Southern Hemisphere midlatitude total wave power. A significant correlation seems to exist in the late 1980s but not in the early 1980s in contrast to the correlation between ozone loss and total wave power, which holds fairly well throughout the 1979–92 period studied. Gray and Ruth (1993) used a two-dimensional model with observed equatorial winds to force the QBO. They proposed a link between the severity of the Antarctic ozone hole and the springtime ozone maximum at Southern Hemisphere midlatitudes in an attempt to resolve discrepancies between the correlation of ozone loss and the QBO in equatorial winds (e.g., Bodeker and Scourfield 1995; Lait et al. 1989). Other studies have suggested that, in addition to the QBO, there may be linkages between South Pacific sea surface temperatures and variations in midlatitude wave activity (Kodera and Yamazaki 1989). We have seen that, in our climate model, the natural variability in tropospheric wave forcing is significant enough to affect ozone loss, possibly accounting for some of the difficulties encountered in previous attempts to correlate ozone loss with the QBO signal only. This work suggests that attempts to predict the severity of the ozone hole based on the phase of the QBO may be confounded by the unforced variability of the atmosphere and that predictions based on midwinter tropospheric wave energy should have some degree of success.

9. Summary

We have studied the interannual variability of the Antarctic ozone hole in the GISS GCM. The model includes the coupled dynamical and radiative responses to the chemical ozone hole. The parameterized chemistry used here results in a simulated ozone hole in good agreement with observations. Zonal mean surface UV flux increases by up to 42%, also in accord with observations. The general temperature response in the

model is radiative cooling in the lower stratosphere, due to the reduction of ozone there, and dynamical warming in the upper stratosphere. There is significant interannual variability in these responses and in the amount of ozone depletion. Total column ozone loss varies by up to 25% interannually, with similar variations in the radiative heating decrease in the lower stratosphere. Dynamically induced heating of the upper stratosphere varies by up to a factor of 3. Temperature and ozone observations show similar variations, though ozone observations show larger maximum variability than that seen here. We find that the interannual differences begin to appear as early as July, before the onset of ozone depletion. They therefore do not result from variations in ozone loss but, instead, are the cause of those variations. We attribute the interannual variability in both dynamical heating and in ozone destruction to differences in the tropospheric wave forcing of the stratosphere and have shown the mechanism by which midwinter variations in wave forcing affect the subsequent propagation of wave energy in the spring. Natural variability of tropospheric wave energy may therefore exert a significant influence on polar dynamics, in addition to periodic forcings such as the solar cycle or the QBO, which we will investigate in future experiments. The current model results support observational correlations that suggest that the observed interannual variation in the severity of the Antarctic ozone hole is driven by variations in midwinter tropospheric wave activity forcing of the stratosphere.

Acknowledgments. D. Shindell gratefully acknowledges support from a NASA EOS Postdoctoral Fellowship. Further support for this research was provided by NASA's Atmospheric Chemistry Modeling Program. Thanks to Patrick Lonergan for assistance with the GCM and to Jean Lerner for assistance with graphics.

REFERENCES

- Austin, J., and N. Butchart, 1992: A three-dimensional modelling study of the influence of planetary wave dynamics on polar ozone photochemistry. *J. Geophys. Res.*, **97**, 10 165–10 186.
- Balachandran, N., and D. Rind, 1995: Modeling the effects of UV variability and the QBO on the troposphere–stratosphere system. Part I: The middle atmosphere. *J. Climate*, **8**, 2058–2079.
- Bodeker, G. E., and M. W. J. Scourfield, 1995: Planetary waves in total ozone and their relation to Antarctic ozone depletion. *Geophys. Res. Lett.*, **22**, 2949–2952.
- Cariolle, D. A., A. Lasserre-Bigorrry, J. F. Royer, and J. F. Geleyn, 1990: A general circulation model simulation of the springtime Antarctic ozone decrease and its impact on mid-latitudes. *J. Geophys. Res.*, **95**, 1883–1898.
- Frederick, J. E., P. F. Soulen, S. B. Diaz, I. Smolskaia, C. R. Booth, T. Lucas, and D. Neuschuler, 1993: Solar ultraviolet irradiance observed from southern Argentina: September 1990 to March 1991. *J. Geophys. Res.*, **98**, 8891–8897.
- Gray, L. J., and S. Ruth, 1993: The modeled latitudinal distribution of the ozone quasi-biennial oscillation using observed equatorial winds. *J. Atmos. Sci.*, **50**, 1033–1046.
- Kawahira, K., and W. Shiratori, 1996: Development and changes of

- the horizontal structure of the ozone hole in Antarctica. *Proc. XVIII Quadrennial Ozone Symp.*, L'Aquila, Italy, Int. Ozone Commission, in press.
- Kiehl, J. T., B. A. Boville, and B. P. Briegleb, 1988: Response of a general circulation model to a prescribed Antarctic ozone hole. *Nature*, **332**, 501–504.
- Kodera, K., and K. Yamazaki, 1989: A possible influence of sea surface temperature variation on the recent development of ozone hole. *J. Meteor. Soc. Japan*, **67**, 465–472.
- Lait, L. R., M. R. Schoeberl, and P. A. Newman, 1989: Quasi-biennial modulation of the Antarctic ozone depletion. *J. Geophys. Res.*, **94**, 11 559–11 571.
- Mahlman, J. D., J. P. Pinto, and L. J. Umscheid, 1994: Transport, radiative, and dynamical effects of the Antarctic ozone hole: A GFDL “SKYHI” model experiment. *J. Atmos. Sci.*, **51**, 489–508.
- Randel, W. J., 1988: The anomalous circulation in the southern hemisphere stratosphere during spring 1987. *Geophys. Res. Lett.*, **15**, 911–914.
- Rind, D., R. Suozzo, N. K. Balachandran, A. Lacis, and G. Russell, 1988a: The GISS global climate/middle atmosphere model. Part I: model structure and climatology. *J. Atmos. Sci.*, **45**, 329–370.
- , —, and —, 1988b: The GISS global climate/middle atmosphere model. Part II: Model variability due to interactions between planetary waves, the mean circulation, and gravity wave drag. *J. Atmos. Sci.*, **45**, 371–386.
- Shindell, D. T., and R. L. de Zafra, 1996: Chlorine monoxide in the Antarctic spring vortex 2. A comparison of measured and modeled diurnal cycling over McMurdo Station, 1993. *J. Geophys. Res.*, **101**, 1475–1487.
- , and —, 1997: Limits on heterogeneous processing in the Antarctic spring vortex from a comparison of measured and modeled chlorine. *J. Geophys. Res.*, **102**, 1441–1450.
- Waters, J. W., L. Froidevaux, G. L. Manney, W. G. Read, and L. S. Elson, 1993: MLS observations of lower stratospheric ClO and O₃ in the 1992 Southern Hemisphere winter. *Geophys. Res. Lett.*, **20**, 1219–1222.
- World Meteorological Organization, 1994: Scientific assessment of ozone depletion. Global Ozone Research and Monitoring Project Rep. 37, Geneva, 451 pp. [Available from Dr. Rumen Bojkov, P.O. Box 2300, 1211-Geneva, Switzerland.]